Letter

Quantum oscillations as a robust fingerprint of chiral anomaly in nonlinear response in Weyl semimetals

Chuanchang Zeng,[1,2] Snehasish Nandy,[3] Pu Liu,[1,2] Sumanta Tewari,[4] and Yugui Yao[1,2,*]

[1]*Centre for Quantum Physics, Key Laboratory of Advanced Optoelectronic Quantum Architecture and Measurement, School of Physics, Beijing Institute of Technology, Beijing, 100081, China*

[2]*Beijing Key Lab of Nanophotonics & Ultrafine Optoelectronic Systems, School of Physics, Beijing Institute of Technology, Beijing, 100081, China*

[3]*Department of Physics, University of Virginia, Charlottesville, Virginia 22904, USA*

[4]*Department of Physics and Astronomy, Clemson University, Clemson, South Carolina 29634, USA*

(Received 10 November 2022; accepted 3 February 2023; published 13 February 2023)

We investigate the nonlinear planar effects (NPEs) in Weyl semimetals (WSMs) starting from the semiclassical regime to the ultraquantum limit within the framework of Boltzmann transport theory incorporating Landau quantization. Based on our results, we propose quantum oscillations in the NPEs as a robust signature of the celebrated chiral anomaly (CA) in WSMs. By obtaining analytical expressions, we show that the quantum oscillations in the nonlinear regime exhibit two different periods in B^{-1} (B is the magnetic field) compared to the linear response regime with only one period in the inverse magnetic field. In addition, we obtain characteristic angular dependence of the CA-induced NPEs. We conclude that in light of the inconclusive sign of the CA-driven longitudinal magnetoconductance in WSMs as has been illustrated in recent theoretical work, the proposed behaviors of quantum oscillations in the nonlinear planar effects uniquely identify the existence of chiral anomaly in WSMs.

DOI: 10.1103/PhysRevB.107.L081107

Introduction. Weyl semimetals (WSMs) have attracted great interest theoretically and experimentally in recent years for offering a plethora of intriguing physical phenomena. Besides the spectroscopic observations of the characteristic Weyl nodes and Fermi arc states, detecting various quantum effects intrinsic to Weyl fermions has also been vastly employed in the identification of the WSMs. Chiral anomaly (CA) or Adler-Bell-Jackiw anomaly is one such intrinsic effect unique to WSMs [1]. In the presence of a nonorthogonal electric and magnetic field, i.e., $\boldsymbol{E}\cdot\boldsymbol{B}\neq 0$, CA pumps charge between Weyl nodes of opposite chirality. This internode flow of charge, balanced with internode scattering with characteristic time τ_v, creates a finite steady-state chiral chemical potential (CCP) μ^C proportional to $\tau_v\boldsymbol{E}\cdot\boldsymbol{B}$, leading to fascinating transport effects. Typical examples are the positive longitudinal magnetoconductivity (LMC) [2,3] along with the planar Hall effect (PHE) [4,5]. Either in the semiclassical regime for small magnetic fields or in the quantum limit with large magnetic fields involving Landau levels, it has been found that the CA-induced longitudinal magnetoconductivity in WSMs is positive and increases with magnetic field $\boldsymbol{B}$ quadratically and linearly, respectively. This renders the measurements of longitudinal magnetoconductivity (i.e., $\boldsymbol{B}||\boldsymbol{J}$, with $\boldsymbol{J}$ the current density), typically small in regular metals because of the absence of Lorentz forces, an important signature of chiral anomaly in WSMs [6–21].

Interestingly, it has recently been reported that not only the LMC and PHE in WSMs can enhance through various extrinsic mechanisms [11,15,22–25] other than CA, but also they can acquire a negative sign as well, either in the semiclassical [26–29] or quantum regime [30–32]. References [33–45] show that the positive LMC and PHE can even appear in materials without any Weyl nodes. As a result, the positive LMC and PHE can no longer be considered sufficient transport signatures for CA, and alternative approaches to identifying the existence of CA in WSMs are highly required [46].

Recent work proposed that a periodic-in-B^{-1} quantum oscillation in the transport coefficients, crossing the semiclassical and ultraquantum limits in the linear response regime, is a unique fingerprint of CA [47–49]. By contrast, in the nonlinear response regime, it has been shown that the transport signatures can be understood as a combined effect of CA and Berry curvature-induced anomalous velocity [50–52] or even purely as a Berry curvature effect [52] within the semiclassical framework. Therefore, a convincing and unambiguous connection between magnetotransport and CA in the nonlinear regime for WSMs is still lacking. In this Letter, we propose a new way to detect CA in WSMs under the action of a moderate magnetic field, via the quantum oscillation in the nonlinear response of LMC and PHE, namely the *nonlinear* planar effects (NPEs). Using Boltzmann transport theory that incorporates Landau quantization, we find that a unique feature of the quantum oscillations of the NPEs is the existence of two different oscillation periods in B^{-1}, one of which remains constant while the other decreases with increasing B^{-1}. We show that these NPE responses rely on the deviations of

*ygyao@bit.edu.cn

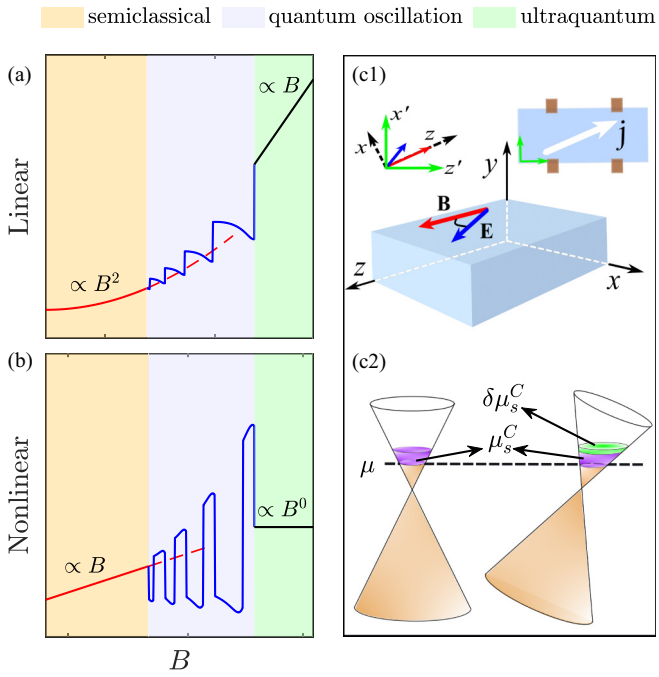

FIG. 1. The phenomenological magnetic field dependence of the linear and nonlinear magneto planar conductivity induced by CA in WSMs are shown in (a) and (b), respectively, for three transport regimes. Panel (c1) presents the geometry of a crossed fields lying in the $x-z$ plane, and the schematic setup for experimental probing (top right, inset) along with the possible coordinate systems (top left, inset). (d) The CA-induced chiral chemical potential (purple, μ_s^C) and its deviation (green, $\delta\mu_s^C$) for a single Weyl cone.

chiral chemical potential, i.e., $\delta\mu^C$, and are directly linked to CA. The quantum oscillation behavior of the NPEs can be contrasted with the CA-driven linear planar effects, which oscillate with only one period in B^{-1}. We also obtain the B-dependent NPE responses in the weak-B limit, consistent with previous semiclassical results [50]. Interestingly, going beyond the semiclassical regime, we find that the NPEs at the ultraquantum limit are magnetic field independent. The comparison of the magnetic field dependencies of CA-induced magnetotransport between the linear [1,2,2,3,47,53–55] and the nonlinear regime is illustrated in Fig. 1. Based on these calculations, we conclude that, in light of the inconclusive sign of the CA-driven longitudinal magnetoconductance in WSMs [26–32], and the existence of such behavior even in the absence of chiral anomaly [33–45], the proposed behaviors of quantum oscillations in the nonlinear planar effects coupled with similar oscillations in the linear response regime, uniquely identify the existence of chiral anomaly in WSMs.

Landau levels of tilted WSMs. The low-energy effective Hamiltonian describing a pair of tilted Weyl nodes can generally be written as

$$H(\boldsymbol{k}) = \sum_s s v_F \hbar \boldsymbol{k}\cdot\boldsymbol{\sigma} + s(\hbar \boldsymbol{w}\cdot\boldsymbol{k} + Q_0)\sigma_0, \qquad (1)$$

where σ_0 and $\boldsymbol{\sigma} = (\sigma_x, \sigma_y, \sigma_z)$ represent Pauli matrices, $s = \pm 1$ is the chirality for each node, v_F denotes the isotropic Fermi velocity in the absence of tilt, and vector $\boldsymbol{w}$ tilts the Weyl node along axis i with strength w_i ($i = x, y, z$). Without loss of generality, a band tilt lying within the yz plane, i.e., $\boldsymbol{w} = (0, w_y, w_z)$ is considered for our discussion hereinafter [56]. A finite energy Q_0, which has been shown earlier [50,51] to be important in generating the nonlinear Hall response induced by CA is also included here.

We proceed by introducing the electromagnetic fields represented by $\mathcal{A} = (\phi, \boldsymbol{A})$ with the vector potential in Landau gauge $\boldsymbol{A} = (0, xB, -E_z t)$ and the scalar potential $\phi = -xE_x$, which yield $\boldsymbol{B} = \nabla \times \boldsymbol{A} = B\hat{\boldsymbol{z}}$ and $\boldsymbol{E} = -\nabla\phi - \partial_t \boldsymbol{A} = (E_x, 0, E_z)$ [57], respectively. Such a configuration is shown in Fig. 1(c1). Following the standard Peierls substitution $\boldsymbol{k} \to \boldsymbol{q} = \boldsymbol{k} + e\boldsymbol{A}/\hbar$, Eq. (1) can be rewritten as

$$H(\boldsymbol{q}) = \sum_s s v_F \hbar \boldsymbol{q}\cdot\boldsymbol{\sigma} + s(\hbar \boldsymbol{w}\cdot\boldsymbol{q} + Q_0)\sigma_0 + exE_x. \qquad (2)$$

It is clear from the Eq. (2) that the band tilt generates an effective electric field $E_{\text{eff}}\hat{\boldsymbol{x}} = s w_y B\hat{\boldsymbol{x}}$ in addition to the external field $E_x\hat{\boldsymbol{x}}$. Now to obtain the Landau levels (LLs), we consider a Lorentz boost along the y axis (perpendicular to $\boldsymbol{E}$ and $\boldsymbol{B}$) in terms of the relativistic parameter β with

$$\beta = \beta_y^w + \beta_x^E, \qquad (3)$$

where $\beta_y^w = s w_y / v_F$ and $\beta_x^E = E_x / v_F B$. Applying this boost transformation and its inverse operation successively, the LLs for Eq. (2) can be obtained as $\varepsilon_n^s(k_y, k_z) = s(Q_0' + w_z \hbar k_z) + s_0 \alpha \sqrt{(v_F \hbar k_z)^2 + 2\alpha|n|(\hbar\omega_c)^2}$, with $s_0 = \text{sgn}(n) = \pm 1$ indicating the nth positive or negative LLs for $|n| \geqslant 1$. Here $\omega_c = v_F/l_B$ with $l_B = \sqrt{\hbar/eB}$ is defined as the cyclotron frequency, characterizing the LL spacing. Factor $\alpha = \sqrt{1-\beta^2}$ indicates the squeezing effect on the LLs as well as the cyclotron frequency. The finite energy Q_0 is now modulated as $Q_0' = Q_0 - s\beta_x^E \hbar k_y$, which incorporates a k_y-dependent band shift brought about by the Lorentz transformation. The zeroth-LL ($n = 0$), similarly, is found as $\varepsilon_0^s(k_y, k_z) = s(Q_0' + w_z k_z - \alpha v_F \hbar k_z)$. With the band dispersion in hand, the longitudinal group velocity $v_{z,n}^s$ for the LLs can be obtained straightforwardly [58]. The LL dispersion for both the tilted and nontilted Weyl node with $s = +1$ is depicted in Fig. 2(a). Obviously, the zeroth-LL dispersing to the right is chiral (in red) while the higher ones are achiral (in blue).

It is important to note that, the motion of the electrons governed by Eq. (2) can be arranged into quantized LLs only within the so-called magnetic regime [59,60], as revealed in previous works either merely when $\beta_x^E < 1$ [47,61–64] or $\beta_y^w < 1$ [56,65,66]. In contrast, here $|\beta| = |\beta_y^w + \beta_x^E| < 1$ is expected to support the quantization. This also implies a more general collapse/breakdown of LLs, which, in our case, is no longer restricted to type-II WSMs [56,65]. As it now depends on the joint effects of the external electric field and band tilt, and hence the LL-collapse can appear even for type-I WSMs.

Boltzmann formalism decorated with Landau quantization. For a single Weyl node with chirality s, the phenomenological Boltzmann transport equation is given by $[\frac{\partial}{\partial t} + \dot{\boldsymbol{r}}^s \cdot \nabla_{\boldsymbol{r}} + \dot{\boldsymbol{k}}^s \cdot \nabla_{\boldsymbol{k}}] f_{\boldsymbol{k},n}^s = \mathcal{I}_{\text{coll}}(f_{\boldsymbol{k},n}^s)$, where $f_{\boldsymbol{k},n}^s$ represents the nonequilibrium Fermi-Dirac distribution function for electrons with energy $\varepsilon_{\boldsymbol{k},n}^s$. We consider the relaxation time approximation for the collision integral $\mathcal{I}_{\text{coll}}(f_{\boldsymbol{k},n}^s)$ that involves both the intranode (τ_a) and internode (τ_v) scattering

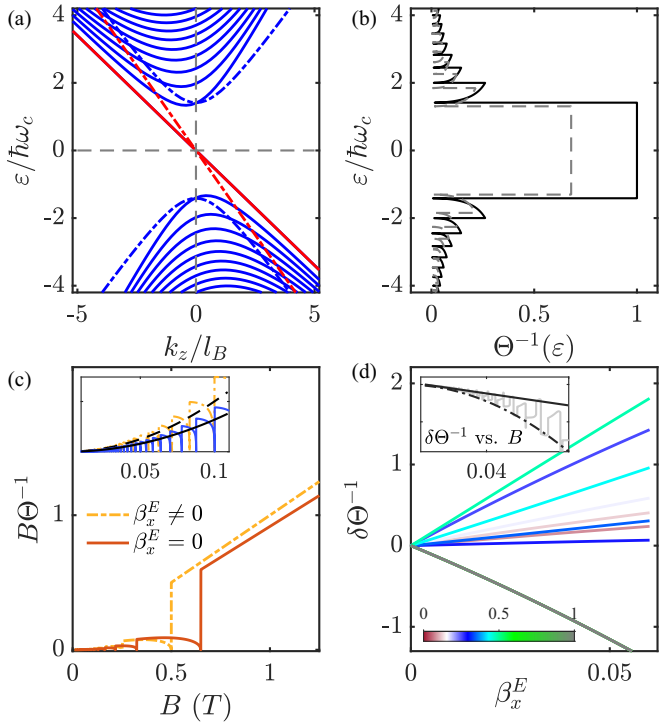

FIG. 2. (a) Landau levels (LLs) projected in the $k_y = 0$ plane for Weyl node $s = +1$, where the solid (dashed) lines represent the LLs of a tilted (nontilted) Weyl node. Panel (b) presents the oscillating DOSs Θ^{-1} as function of Fermi energy. The dashed (solid) curves imply for the case with $\beta s \neq 0$, i.e., $\beta_x^E = 0.1$, $\beta_y^w = 0.1$ ($\beta s = 0$, i.e., $\beta_x^E = \beta_y^w = 0$). To better reveal the modification, here a finite $w_z = 0.3$ is taken for the case with $\beta_s \neq 0$. Panel (c) plots $B\Theta^{-1}$ as function of B, where the inset shows the quadratic-in-B dependence in the weak-B limit. (d) The linear dependency of $\delta\Theta^{-1}$ on β_x^E at various magnetic field strengths (indicated by the color scale). The inset shows $\delta\Theta^{-1} \propto B$ in the weak-B limit.

processes in WSMs. Specifically, the scattering time τ_a relaxes the electron from $f^s_{\boldsymbol{k},n}$ to a local equilibrium state $f^s_{\rm eq}$, while τ_v indicates the relaxation to a global equilibrium state $f^0_{\rm eq}$. It is worthy to note that we have $\langle f^s_{\boldsymbol{k},n}\rangle_s = f^s_{\rm eq}$, with $\langle\rangle_s$ averaging over all the possible electron states [47,52].

Solving the Boltzmann equation in the current setup [58], the energy deviation $\delta\varepsilon^s_{\boldsymbol{k},n}$ perturbed by fields can be obtained as $\delta\varepsilon^s_{\boldsymbol{k},n} = -\tau_a e\boldsymbol{E}\cdot\boldsymbol{v}^s_{\boldsymbol{k},n} + (1-\tau_a/\tau_v)\mu^C_s$, with μ^C_s given as

$$\mu^C_s = \mu_s - \mu = -\tau_v e\langle \boldsymbol{E}\cdot\boldsymbol{v}^s_{\boldsymbol{k},\boldsymbol{n}}\rangle_s, \tag{4}$$

exactly the CA-induced CCP for the Weyl node with chirality s. In the geometry of $\boldsymbol{E}\cdot\boldsymbol{B} \neq 0$ lying in the $x-z$ plane, the longitudinal ($\parallel$ with $\boldsymbol{B}$) charge current is found to be $\boldsymbol{j}_z = \boldsymbol{j}^C_z + \boldsymbol{j}^N_z$, i.e., composed of the CA-induced response $\boldsymbol{j}^C_z$ and the normal drift response $\boldsymbol{j}^N_z$, respectively written as

$$\boldsymbol{j}^C_z = c_0 v_F(\tau_v - \tau_a)\frac{E_z B}{\mathcal{F}_\Theta}, \quad \boldsymbol{j}^N_z = c_0 v_F \tau_a \mathcal{F}_\Lambda E_z B \tag{5}$$

with $c_0 = 2e^3/h^2$. The auxiliary function $\mathcal{F}_x$ here is defined as $\mathcal{F}_x = \int d\varepsilon[-\partial_\varepsilon f_0(\varepsilon)]x(\varepsilon)$, with $x = \Theta(\varepsilon)$, $\Lambda(\varepsilon)$ (see the details in the Supplementary Material [58]). In the zero-temperature limit where the quantized LLs are not smeared from temperature broadening effect [58], we have $-\partial_\varepsilon f_0(\varepsilon) = \delta(\varepsilon-\varepsilon_F)$, such that functions $\mathcal{F}_\Theta$, $\mathcal{F}_\Lambda$ are respectively reduced to $\mathcal{F}_\Theta = \Theta(\varepsilon_F)$, $\mathcal{F}_\Lambda = \Lambda(\varepsilon_F)$.

We want to mention that $\Theta(\varepsilon)$, as plotted in Fig. 2(b), is in effect the density of states (DOSs) for a single Weyl cone at energy ε, which can be modulated by the presence of different fields. While $\Lambda(\varepsilon)$ (i.e., $\mathcal{F}_\Lambda$) presents evident oscillations even with much bigger amplitudes than that of $\Theta(\varepsilon)$ [58], the manifested oscillations of $\boldsymbol{j}_z$ will be mainly determined by $\Theta(\varepsilon)$. This is because of the large ratio of scattering timescales τ_v/τ_a in WSMs. For instance, based on $\tau_v/\tau_a \sim (2k_0/k_F)^4$ with $2k_0$ the Weyl node separation and k_F the Fermi wave vector [67], this ratio can be estimated as $\tau_v/\tau_a \sim 10^4$ in WSM Na_3Bi [68].

After some algebra with Eqs. (4) and (5), the CA-induced response can be found to be $\boldsymbol{j}^C_z \propto B\mu^C_s$, where $\mu^C_s = s\tau_v e E_z v_F/\Theta$ is the CCP, chirality dependent as expected for each Weyl node. Straightforwardly, a charge current linear in E_z is obtainable. The magnetic field dependency of j^C_z is revealed by Fig. 2(c), where a quadratic-in-$\boldsymbol{B}$ (inset) and linear-in-$\boldsymbol{B}$ signature is observed in the weak and strong field limits, respectively. This directly recovers the conventional result as discussed for the linear magnetotransports in earlier studies [2–4], and more relevant discussions can be found in the Supplementary Material [58]. Next, we will investigate the CA-induced NPEs.

Chiral anomaly-induced nonlinear transports. As shown in Figs. 2(b) and 2(c), the DOSs Θ (or Θ^{-1}) get modified when $\beta^E_x \neq 0$ or/and $\beta^w_y \neq 0$ compared to the nonperturbed case. Such modification turns out to be responsible for the nonlinear CA-related responses. In effect, the transverse component $E_x\hat{\boldsymbol{x}}$ (as $\beta^E_x \neq 0$) can bring in additional E dependence for the generated CCP in WSMs besides the longitudinal $E_z\hat{\boldsymbol{z}}$, making the CA-induced nonlinear responses possible. Considering this, we can formulate the charge current $\boldsymbol{j}_z$ as $\boldsymbol{j}_z = \sigma_{zz}E_z + \chi_{zzx}E_zE_x + \cdots$, where σ_{zz} and χ_{zzx} are the linear and second-order nonlinear conductivity tensors, respectively. Based on Eq. (5), it is clear that σ_{zz} and χ_{zzx} are fully determined by $\Theta(\varepsilon)$, $\Lambda(\varepsilon)$.

Irrespective of the particular magnetic field regime, it is allowed to expand Θ^{-1} in terms of β^E_x perturbatively to study the effect of β^E_x, which can be given as

$$\Theta^{-1}(\varepsilon) = \Theta_0^{-1}(\varepsilon) + \beta^E_x\Theta_r^{-1}(\varepsilon) + \mathcal{O}\big[\big(\beta^E_x\big)^2\big]. \tag{6}$$

The above expansion is valid as long as $\beta^E_x \ll 1$ is satisfied (similarly, for $\Lambda(\varepsilon)$ we have Λ_0, Λ_r [58]). As such, Θ_0^{-1}, Θ_r^{-1} are E_x independent. The modifications denoted as $\delta\Theta^{-1} = \Theta^{-1} - \Theta_0^{-1}$ (similarly $\delta\Lambda$), as expected from Eq. (6), are found to be roughly linear in β^E_x under various magnetic fields at the limit of $\beta^E_x \ll 1$, which now are given in Fig. 2(d). Additionally, a linear dependency of $\delta\Theta^{-1}$ in $\boldsymbol{B}$ is also observed in the weak field regime (black solid line, inset).

Recapping $\mu^C_s \propto E_z\Theta^{-1}$ and $\boldsymbol{j}_z \propto BE_z\Theta^{-1}$, one obtains

$$\mu^C_s(\varepsilon) = \mu^C_{s,0}(\varepsilon) + \delta\mu^C_s(\varepsilon). \tag{7}$$

Here $\mu^C_{s,0}(\varepsilon) \propto E_z\Theta_0^{-1}$ denotes the conventional CCP that governs the linear magneto transports in WSMs, i.e., $\sigma_{zz} \propto \mu^C_{s,0} \propto \Theta_0^{-1}$. On the other hand, we also have $\delta\mu^C_s(\varepsilon) \propto E_z\beta^E_x\Theta_r^{-1}$ for the the deviation of CCP, which exactly gives rise to the second-order nonlinear responses. A comparison

between μ_s^C and $\delta\mu_s^C$ is schematically shown in Fig. 1(c2). Based on the above analysis, the nonlinear conductivity χ_{zzx} can be obtained as

$$\chi_{zzx} = c_0\big[(\tau_v - \tau_a)\Theta_r^{-1}(\varepsilon) + \tau_a\Lambda_r(\varepsilon)\big]. \tag{8}$$

Hereafter, $\sum_s$ is omitted for simplicity. Note that all the field dependencies of the conductivity will be solely revealed by functions Θ_r^{-1}, Λ_r, and Θ_r^{-1} explicitly appears in $\delta\mu_s^C$, connecting with the CA in WSMs unambiguously.

Moving to the semiclassical regime with $\varepsilon_F \gg \hbar\omega_c$ (i.e., weak magnetic field regime) where the LL description is not valid, the CA-induced and the normal-drift-contributed nonlinear conductivity can be obtained based on Eq. (8) as [58]

$$\chi_{zzx}^C \propto w_y^s\tau_v B/\tilde{\varepsilon}_s^2, \quad \chi_{zzx}^N \propto w_y^s\tau_a\tilde{\varepsilon}_s^2/B, \tag{9}$$

respectively. Here $\tilde{\varepsilon}_s = (\varepsilon - sQ_0)/v_F\hbar$, $w_y^s = sw_y/v_F$, and approximations $|\beta_x^E|^2 \ll 1$, $|\beta_y^w|^2 \ll 1$ have been applied in the derivations. Note that the different parameter dependencies between χ_{zzx}^C and χ_{zzx}^N are helpful to distinguish their contribution to the nonlinear response, though typically the former, i.e., CA, will be the leading contributor in WSMs due to $\tau_v/\tau_a \gg 1$. It is also interesting to notice that the CA-induced nonlinear conductivity tensor in the semiclassical regime is linear in magnetic field, in contrast to that of the linear transports. This also makes the CA-induced nonlinear response easily distinguished from other possible plaguing effects [15,22–24].

Similarly, the conductivity tensor in the ultraquantum regime with $\hbar\omega_c \gg \varepsilon_F$ can be obtained as

$$\chi_{zzx}^C \propto w_y^s\tau_v, \quad \chi_{zzx} \approx \chi_{zzx}^C. \tag{10}$$

In this regime, only the chiral zeroth-LL is occupied due to the large LL spacing under the strong magnetic field. Interestingly, χ_{zzx} is magnetic field-independent as well as Fermi energy-independent in this regime, different from that in the semiclassical limit. As a result, the CA-induced nonlinear responses can survive under the strong magnetic field only for the pair of achirally tilted Weyl nodes ($w_y^+ \neq -w_y^-$).

Note that the nonlinear conductivity discussed above explicitly depends on the band tilt, thus clearly implying a joint effect of the transverse electric field and the band tilt. Specifically, the nonlinear current is given by $\boldsymbol{j}_z \propto \tau_v w_y^s E_x E_z B$, which can be effectively provided by $(\boldsymbol{E}\cdot\boldsymbol{B})(\boldsymbol{E}\times\boldsymbol{w})$, exactly the configuration employed for the CA-induced nonlinear transport effects in recent works [50–52].

Signatures for experimental probing. It is now known that quantum oscillation effects origin from the successive crossing of the Fermi energy by LLs, which manifests as the periodic change in the electron or hole DOSs [69]. As shown in Fig. 2(b), the amplitudes of $\Theta^{-1}(\varepsilon)$ drops down to zero periodically, attributing to the Van Hove singularities in $\Theta(\varepsilon)$ at $\varepsilon_F = \sqrt{2|n|\alpha(1-\beta'^2)(\hbar\omega_c)^2}$ (i.e., infinitely large DOSs, see in Ref. [58]). This feature is also present in CCP as well as the magneto conductivity in WSMs, for which the oscillating period can be obtained as

$$\Delta(B^{-1}) = 2\alpha(1-\beta'^2)(v_F\hbar/\varepsilon_F)^2 e/\hbar. \tag{11}$$

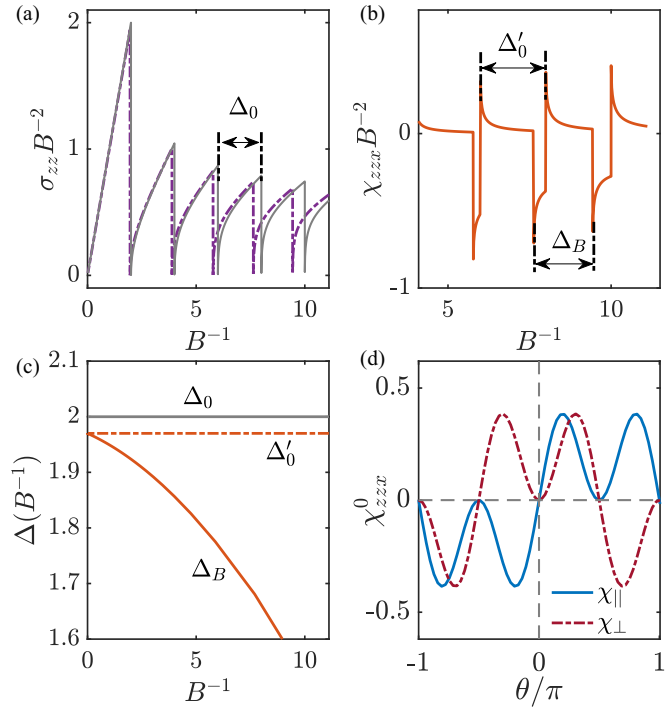

FIG. 3. Periodic oscillations in B^{-1} of the linear (σ_{zz}) and nonlinear conductivity (χ_{zzx}) in panels (a) and (b), respectively. Note that the additional β_x^E does not make big difference on the magnitudes of σ_{zz}. The constant periods Δ_0, Δ_0' and the magnetic field dependent Δ_B are compared in panel (c). Here $E_F = v_F\sqrt{e\hbar}(= 1\hbar\omega_c|_{B=1})$ is taken. Panel (d) presents the angular dependencies of the longitudinal ($\chi_{||}$) and transverse ($\chi_\perp$) components of the magneto conductivity tensor, here $\theta = \langle \boldsymbol{E}, \boldsymbol{B}\rangle$ as shown in Fig. 1.

Here $\beta' = \sqrt{\beta^2 + (\beta_z^w)^2}$ with $\beta_z^w = sw_z/v_F$ accounting the band tilt along z direction. As the value of w_z only changes the relative magnitudes of the oscillating quantities, here for simplicity we consider the case of $w_y \neq 0$, $w_z = 0$. Thus, the period is simply given as $\Delta(B^{-1}) = 2\alpha^3(v_F\hbar/\varepsilon_F)^2 e/\hbar$, which obtains modification from factor α^3.

As shown in Fig. 3(a), $\sigma_{zz}B^{-2}$ is plotted as a function of B^{-1}, showing that a finite β_x^E leads to a decreasing oscillating period (dashed line), in contrast to the case of $\beta_x^E = 0$ with the period being a constant (gray solid, Δ_0). Interestingly, since the second-order nonlinear transports link with $\delta\mu_s^C$, which as discussed earlier is proportional to $(\Theta^{-1} - \Theta_0^{-1})$, the corresponding conductivity $\chi_{zzx}B^{-2}$ can reveal two different oscillating periods simultaneously. As shown in Fig. 3(b), one period remains as a constant Δ_0' due to Θ_0^{-1}, while the other one Δ_B corresponding to Θ^{-1} exhibits an evident magnetic field dependency. The above-mentioned oscillation periods are shown in Fig. 3(c) for comparison. Note that the difference between Δ_0 and Δ_0' depends on the exact value of β_y^w, and the decreasing period appears as long as the transverse electric field ($\beta_x^E \neq 0$) is present. We want to point out that such a remarkable oscillating feature, different from all the known quantum oscillation effects, is characteristic of the CA-induced second-order nonlinear transports.

Besides the oscillation periods, angular dependence is another probable signature that is important in studying

the CA-related transports in WSMs. Though the longitudinal charge currents (and conductivity tensors) are written to be locked to $\boldsymbol{B} = B\hat{z}$, it naturally gives rise to the planar transport components when expressed in terms of the crystal axes or the orthogonal directions with respect to $\boldsymbol{E}$ ($\langle \boldsymbol{E}, \boldsymbol{B} \rangle = \theta$, see Fig. 1). As has been discussed for the linear transports [55,57], one can obtain $\sigma_{||} = \sigma_{zz} \cos^2\theta, \sigma_{\perp} = \sigma_{zz} \cos\theta \sin\theta$ as the LMC and PHE conductivity tensor, respectively.

In the nonlinear transports, we have $\chi_{||} = \chi_{zzx} \cos^2\theta \sin\theta$ and $\chi_{\perp} = \chi_{zzx} \sin^2\theta \cos\theta$, which can be taken as CA-induced nonlinear LMC and PHE tensors, respectively. The angular dependencies for $\chi_{||}$, $\chi_{\perp}$ are now plotted in Fig. 3(d). Interestingly, all the NPE conductivity tensors switch signs when changing the angle θ, and the nonlinear LMC is odd while the PHE is even in θ. These features of NPEs are fundamentally different from that in the linear transport regime and hence are helpful for the probing of the CA-induced NPEs in experiments. The angular dependencies of the NPEs are also expected to be free of any squeezing effects and thus robust for experimental probing, in contrast to the linear case where a closer angular dependency $\cos^4\theta$ [9,46,70] or $\cos^6\theta$ [57] was found for LMC instead of the predicted $\cos^2\theta$. Additionally, the CA-induced NPEs discussed in this work are measurable through frequency lock-in measurement using AC current, as has been conducted successfully in experiments for other nonlinear effects [71–73].

Conclusion. By considering the configuration with noncollinear electric and magnetic field and simultaneously involving a band tilt, we show that, besides the fascinating angular dependence, the CA-induced NPEs for WSMs display unique quantum oscillation features in the intermediate magnetic field regime. Specifically, in striking contrast to the oscillations with a single period in B^{-1} obtained for the positive LMC and PHE in the linear transport regime [47,55,57,64,66], the CA-induced NPEs exhibit quantum oscillations with two different period scales, one remaining constant while the other decreasing with increasing B^{-1}. We show that such behaviors are directly connected to chiral anomaly through the deviation in the chiral chemical potential, thereby making the characteristic quantum oscillation signatures in the nonlinear and linear response regimes uniquely suitable for identifying CA in WSMs.

Acknowledgments. The work is supported by the National Key R&D Program of China (Grant No. 2020YFA0308800), the NSF of China (Grants No. 12104043, No. 11734003, and No. 12061131002), the Strategic Priority Research Program of Chinese Academy of Sciences (Grant No. XDB30000000), and the fellowship of the China Postdoctoral Science Foundation (Grant No. 2021M690409). S.N. acknowledges the National Science Foundation Grant No. DMR-1853048. S.T. thanks the ARO Grant No. W911NF-16-1-0182 and Grant No. NSF2014157 for support. C.Z. also thanks J. M. Shao for the useful discussions.

[1] H. Nielsen and M. Ninomiya, Phys. Lett. B **130**, 389 (1983).
[2] D. T. Son and B. Z. Spivak, Phys. Rev. B **88**, 104412 (2013).
[3] A. A. Burkov, Phys. Rev. Lett. **113**, 247203 (2014).
[4] A. A. Burkov, Phys. Rev. B **96**, 041110(R) (2017).
[5] S. Nandy, G. Sharma, A. Taraphder, and S. Tewari, Phys. Rev. Lett. **119**, 176804 (2017).
[6] L. P. He, X. C. Hong, J. K. Dong, J. Pan, Z. Zhang, J. Zhang, and S. Y. Li, Phys. Rev. Lett. **113**, 246402 (2014).
[7] T. Liang, Q. Gibson, M. N. Ali, M. Liu, R. J. Cava, and N. P. Ong, Nat. Mater. **14**, 280 (2015).
[8] Q. Li, D. E. Kharzeev, C. Zhang, Y. Huang, I. Pletikosić, A. V. Fedorov, R. D. Zhong, J. A. Schneeloch, G. D. Gu, and T. Valla, Nat. Phys. **12**, 550 (2016).
[9] C.-L. Zhang, S.-Y. Xu, I. Belopolski, Z. Yuan, Z. Lin, B. Tong, G. Bian, N. Alidoust, C.-C. Lee, S.-M. Huang *et al.*, Nat. Commun. **7**, 10735 (2016).
[10] M. Hirschberger, S. Kushwaha, Z. Wang, Q. Gibson, S. Liang, C. A. Belvin, B. A. Bernevig, R. J. Cava, and N. P. Ong, Nat. Mater. **15**, 1161 (2016).
[11] Y. Li, Z. Wang, P. Li, X. Yang, Z. Shen, F. Sheng, X. Li, Y. Lu, Y. Zheng, and Z.-A. Xu, Front. Phys. **12**, 127205 (2017).
[12] E. Zhang, R. Chen, C. Huang, J. Yu, K. Zhang, W. Wang, S. Liu, J. Ling, X. Wan, H.-Z. Lu, and F. Xiu, Nano Lett. **17**, 878 (2017).
[13] N. Kumar, S. N. Guin, C. Felser, and C. Shekhar, Phys. Rev. B **98**, 041103(R) (2018).
[14] F. C. Chen, X. Luo, J. Yan, Y. Sun, H. Y. Lv, W. J. Lu, C. Y. Xi, P. Tong, Z. G. Sheng, X. B. Zhu, W. H. Song, and Y. P. Sun, Phys. Rev. B **98**, 041114(R) (2018).
[15] S. Liang, J. Lin, S. Kushwaha, J. Xing, N. Ni, R. J. Cava, and N. P. Ong, Phys. Rev. X **8**, 031002 (2018).
[16] M. Wu, G. Zheng, W. Chu, Y. Liu, W. Gao, H. Zhang, J. Lu, Y. Han, J. Zhou, W. Ning, and M. Tian, Phys. Rev. B **98**, 161110(R) (2018).
[17] S.-B. Zhang and J. Zhou, Phys. Rev. B **101**, 085202 (2020).
[18] F. Xiong, C. Honerkamp, D. M. Kennes, and T. Nag, Phys. Rev. B **106**, 045424 (2022).
[19] S.-B. Zhang, H.-Z. Lu, and S.-Q. Shen, New J. Phys. **18**, 053039 (2016).
[20] J. Hofmann, Phys. Rev. B **100**, 245140 (2019).
[21] J. Hofmann and S. Das Sarma, Phys. Rev. B **93**, 241402(R) (2016).
[22] F. Arnold, C. Shekhar, S.-C. Wu, Y. Sun, R. D. Dos Reis, N. Kumar, M. Naumann, M. O. Ajeesh, M. Schmidt, A. G. Grushin, J. H. Bardarson, M. Baenitz, D. Sokolov, H. Borrmann, M. Nicklas, C. Felser, E. Hassinger, and B. Yan, Nat. Commun. **7**, 11615 (2016).
[23] R. D. dos Reis, M. O. Ajeesh, N. Kumar, F. Arnold, C. Shekhar, M. Naumann, M. Schmidt, M. Nicklas, and E. Hassinger, New J. Phys. **18**, 085006 (2016).
[24] J. Yang, W. L. Zhen, D. D. Liang, Y. J. Wang, X. Yan, S. R. Weng, J. R. Wang, W. Tong, L. Pi, W. K. Zhu, and C. J. Zhang, Phys. Rev. Mater. **3**, 014201 (2019).
[25] A. Yamada and Y. Fuseya, Phys. Rev. B **105**, 205207 (2022).
[26] A. Knoll, C. Timm, and T. Meng, Phys. Rev. B **101**, 201402(R) (2020).
[27] C. Xiao, H. Chen, Y. Gao, D. Xiao, A. H. MacDonald, and Q. Niu, Phys. Rev. B **101**, 201410(R) (2020).

[28] G. Sharma, S. Nandy, and S. Tewari, Phys. Rev. B **102**, 205107 (2020).

[29] A. Ahmad and G. Sharma, Phys. Rev. B **103**, 115146 (2021).

[30] H.-Z. Lu, S.-B. Zhang, and S.-Q. Shen, Phys. Rev. B **92**, 045203 (2015).

[31] C.-Z. Chen, H. Liu, H. Jiang, and X. C. Xie, Phys. Rev. B **93**, 165420 (2016).

[32] X. Li, B. Roy, and S. Das Sarma, Phys. Rev. B **94**, 195144 (2016).

[33] S. Wiedmann, A. Jost, B. Fauqué, J. van Dijk, M. J. Meijer, T. Khouri, S. Pezzini, S. Grauer, S. Schreyeck, C. Brüne, H. Buhmann, L. W. Molenkamp, and N. E. Hussey, Phys. Rev. B **94**, 081302(R) (2016).

[34] X. Dai, Z. Z. Du, and H.-Z. Lu, Phys. Rev. Lett. **119**, 166601 (2017).

[35] B. A. Assaf, T. Phuphachong, E. Kampert, V. V. Volobuev, P. S. Mandal, J. Sánchez-Barriga, O. Rader, G. Bauer, G. Springholz, L. A. de Vaulchier, and Y. Guldner, Phys. Rev. Lett. **119**, 106602 (2017).

[36] A. V. Andreev and B. Z. Spivak, Phys. Rev. Lett. **120**, 026601 (2018).

[37] D. Rakhmilevich, F. Wang, W. Zhao, M. H. W. Chan, J. S. Moodera, C. Liu, and C.-Z. Chang, Phys. Rev. B **98**, 094404 (2018).

[38] G. Yin, J.-X. Yu, Y. Liu, R. K. Lake, J. Zang, and K. L. Wang, Phys. Rev. Lett. **122**, 106602 (2019).

[39] I. Groen, V. T. Pham, N. Leo, A. Marty, L. E. Hueso, and F. Casanova, Phys. Rev. Appl. **15**, 044010 (2021).

[40] J. Li, S. L. Li, Z. W. Wu, S. Li, H. F. Chu, J. Wang, Y. Zhang, H. Y Tian, and D. N. Zheng, J. Phys.: Condens. Matter **22**, 146006 (2010).

[41] K. M. Seemann, F. Freimuth, H. Zhang, S. Blügel, Y. Mokrousov, D. E. Bürgler, and C. M. Schneider, Phys. Rev. Lett. **107**, 086603 (2011).

[42] A. A. Taskin, H. F. Legg, F. Yang, S. Sasaki, Y. Kanai, K. Matsumoto, A. Rosch, and Y. Ando, Nat. Commun. **8**, 1340 (2017).

[43] S. Nandy, A. Taraphder, and S. Tewari, Sci. Rep. **8**, 14983 (2018).

[44] S.-H. Zheng, H.-J. Duan, J.-K. Wang, J.-Y. Li, M.-X. Deng, and R.-Q. Wang, Phys. Rev. B **101**, 041408(R) (2020).

[45] A. Bhardwaj, S. Prasad P., K. V. Raman, and D. Suri, Appl. Phys. Lett. **118**, 241901 (2021).

[46] N. P. Ong and S. Liang, Nat. Rev. Phys. **3**, 394 (2021).

[47] M.-X. Deng, G. Y. Qi, R. Ma, R. Shen, R.-Q. Wang, L. Sheng, and D. Y. Xing, Phys. Rev. Lett. **122**, 036601 (2019).

[48] C.-L. Zhang, B. Tong, Z. Yuan, Z. Lin, J. Wang, J. Zhang, C.-Y. Xi, Z. Wang, S. Jia, and C. Zhang, Phys. Rev. B **94**, 205120 (2016).

[49] J. Du, H. Wang, Q. Chen, Q. Mao, R. Khan, B. Xu, Y. Zhou, Y. Zhang, J. Yang, B. Chen, C. Feng, and M. Fang, Sci. China: Phys., Mech. Astron. **59**, 5798 (2016).

[50] R.-H. Li, O. G. Heinonen, A. A. Burkov, and Steven S.-L. Zhang, Phys. Rev. B **103**, 045105 (2021).

[51] S. Nandy, C. Zeng, and S. Tewari, Phys. Rev. B **104**, 205124 (2021).

[52] C. Zeng, S. Nandy, and S. Tewari, Phys. Rev. B **105**, 125131 (2022).

[53] A. A. Zyuzin and A. A. Burkov, Phys. Rev. B **86**, 115133 (2012).

[54] E. V. Gorbar, V. A. Miransky, and I. A. Shovkovy, Phys. Rev. B **89**, 085126 (2014).

[55] K. Das, S. K. Singh, and A. Agarwal, Phys. Rev. Res. **2**, 033511 (2020).

[56] S. Tchoumakov, M. Civelli, and M. O. Goerbig, Phys. Rev. Lett. **117**, 086402 (2016).

[57] M.-X. Deng, H.-J. Duan, W. Luo, W. Y. Deng, R.-Q. Wang, and L. Sheng, Phys. Rev. B **99**, 165146 (2019).

[58] See Supplemental Material at http://link.aps.org/supplemental/10.1103/PhysRevB.107.L081107 for the relevant discussions in detail, which includes Refs. [2,32,47,48,56,57,61–66,74–79].

[59] J. D. Jackson, *Classical Electrodynamics* (Wiley, New York, 1998).

[60] L. D. Landau and E. M. Lifshitz, *The Classical Theory of Fields* (Pergamon Press, Oxford, UK, 1971).

[61] V. Lukose, R. Shankar, and G. Baskaran, Phys. Rev. Lett. **98**, 116802 (2007).

[62] N. M. R. Peres and E. V. Castro, J. Phys.: Condens. Matter **19**, 406231 (2007).

[63] V. Arjona, E. V. Castro, and M. A. H. Vozmediano, Phys. Rev. B **96**, 081110(R) (2017).

[64] M.-X. Deng, J.-Y. Ba, R. Ma, W. Luo, R.-Q. Wang, L. Sheng, and D. Y. Xing, Phys. Rev. Res. **2**, 033346 (2020).

[65] Z.-M. Yu, Y. Yao, and S. A. Yang, Phys. Rev. Lett. **117**, 077202 (2016).

[66] J. Shao and L. Yan, J. Phys.: Condens. Matter **33**, 185704 (2021).

[67] S. A. Parameswaran, T. Grover, D. A. Abanin, D. A. Pesin, and A. Vishwanath, Phys. Rev. X **4**, 031035 (2014).

[68] Z. K. Liu, B. Zhou, Y. Zhang, Z. J. Wang, H. M. Weng, D. Prabhakaran, S. K. Mo, Z. X. Shen, Z. Fang, X. Dai, Z. Hussain, and Y. L. Chen, Science **343**, 864 (2014).

[69] N. Brandt, S. Chudinov, and Y. Ponovarev (eds.), *Semimetals*, Modern Problems in Condensed Matter Sciences (Elsevier, Amsterdam, 1988), Vol. 20, pp. 109–128.

[70] J. Xiong, S. K. Kushwaha, T. Liang, J. W. Krizan, M. Hirschberger, W. Wang, R. J. Cava, and N. P. Ong, Science **350**, 413 (2015).

[71] K. Kang, T. Li, E. Sohn, J. Shan, and K. F. Mak, Nat. Mater. **18**, 324 (2019).

[72] Q. Ma, S.-Y. Xu, H. Shen, D. MacNeill, V. Fatemi, T.-R. Chang, A. M. Mier Valdivia, S. Wu, Z. Du, C.-H. Hsu, S. Fang, Q. D. Gibson, K. Watanabe, T. Taniguchi, R. J. Cava, E. Kaxiras, H.-Z. Lu, H. Lin, L. Fu, N. Gedik *et al.*, Nature (London) **565**, 337 (2019).

[73] S. Lai, H. Liu, Z. Zhang, J. Zhao, X. Feng, N. Wang, C. Tang, Y. Liu, K. S. Novoselov, S. A. Yang, and W.-b. Gao, Nat. Nanotechnol. **16**, 869 (2021).

[74] M. Udagawa and E. J. Bergholtz, Phys. Rev. Lett. **117**, 086401 (2016).

[75] R. M. A. Dantas, F. Peña-Benitez, B. Roy, and P. Surówka, J. High Energy Phys. 12 (2018) 069.

[76] X. Xiao, K. T. Law, and P. A. Lee, Phys. Rev. B **96**, 165101 (2017).

[77] R. Gammag and C. Villagonzalo, Solid State Commun. **146**, 487 (2008).

[78] A. Gupta, Phys. Lett. A **383**, 2339 (2019).

[79] A. Menon and B. Basu, J. Phys.: Condens. Matter **33**, 045602 (2021).